Mg substitution effect on the hydrogenation behaviour, thermodynamic and structural properties of the La$_2$Ni$_7$–H(D)$_2$ system

R.V. Denys[a,b], A.B. Riabov[a,b], V.A. Yartys[a,*], Masashi Sato[c], R.G. Delaplane[a,d,1]

[a]*Institute for Energy Technology, P.O. Box 40, Kjeller NO 2027, Norway*
[b]*Physico-Mechanical Institute of the National Academy of Science of Ukraine, 5 Naukova St., Lviv 79601, Ukraine*
[c]*Department of Applied Chemistry, School of Engineering, Tokai University, 1117 Kita-Kaname, Hiratsuka, Kanagawa 259-1292, Japan*
[d]*The Studsvik Neutron Research Laboratory, Uppsala University, S-611 82 Nyköping, Sweden*

Abstract

The present work is focused on studies of the influence of magnesium on the hydrogenation behaviour of the $(La,Mg)_2Ni_7$ alloys. Substitution of La in La$_2$Ni$_7$ by Mg to form La$_{1.5}$Mg$_{0.5}$Ni$_7$ preserves the initial Ce$_2$Ni$_7$ type of the hexagonal $P6_3/mmc$ structure and leads to contraction of the unit cell. The system La$_{1.5}$Mg$_{0.5}$Ni$_7$–H$_2$ (D$_2$) was studied using *in situ* synchrotron X-ray and neutron powder diffraction in H$_2$/D$_2$ gas and pressure–composition–temperature measurements. La replacement by Mg was found to proceed in an ordered way, only within the Laves-type parts of the hybrid crystal structure, yielding formation of LaMgNi$_4$ slabs with statistic and equal occupation of one site by La and Mg atoms. Mg alters structural features of the hydrogenation process. Instead of a strong unilateral anisotropic expansion which takes place on hydrogenation of La$_2$Ni$_7$, the unit cell of La$_{1.5}$Mg$_{0.5}$Ni$_7$D$_{9.1}$ is formed by nearly equal hydrogen-induced expansions proceeding in the basal plane ($\Delta a/a = 7.37\%$) and along [001] ($\Delta c/c = 9.67\%$). In contrast with La$_2$Ni$_7$D$_{6.5}$ where only LaNi$_2$ layers absorb hydrogen atoms, in La$_{1.5}$Mg$_{0.5}$Ni$_7$D$_{9.1}$ both LaNi$_5$ and LaMgNi$_4$ layers become occupied. Nine types of sites were found to be filled by D in total, including tetrahedral $(La,Mg)_2Ni_2$, $(La,Mg)Ni_3$, Ni$_4$, tetragonal pyramidal La$_2$Ni$_3$ and trigonal bipyramidal $(La,Mg)_3Ni_2$ interstices. The hydrogen sublattice around the La/Mg site shows formation of two co-ordination spheres of D atoms: an octahedron MgD$_6$ and a 16-vertex polyhedron LaD$_{16}$ around La. The interatomic distances are in the following ranges: La–D (2.28–2.71), Mg–D (2.02–2.08), Ni–D (1.48–1.86 Å). All D–D distances exceed 1.9 Å. Thermodynamic PCT studies yielded the following values for the ΔH and ΔS of hydrogenation/decomposition; $\Delta H_H = -15.7 \pm 0.9\,\text{kJ}\,(\text{mol}_H)^{-1}$ and $\Delta S_H = -46.0 \pm 3.7\,\text{J}\,(\text{K}\,\text{mol}_H)^{-1}$ for H$_2$ absorption, and $\Delta H_H = 16.8 \pm 0.4\,\text{kJ}\,(\text{mol}_H)^{-1}$ and $\Delta S_H = 48.1 \pm 1.5\,\text{J}\,(\text{K}\,\text{mol}_H)^{-1}$ for H$_2$ desorption.
© 2008 Elsevier Inc. All rights reserved.

Keywords: Metal hydrides; Crystal structure and symmetry; Neutron diffraction; Pressure-composition-temperature relationships

1. Introduction

The crystal structures of the intermetallic alloys formed in the systems of rare-earth metals (A) with Ni or Co (B), have numerous representatives formed between compositions AB_2 (Laves compounds) and AB_5 (Haucke phases). Their composition AB_a ($2 < a < 5$) can be presented as a combination of $n\,AB_5$ and $m\,A_2B_4$ units. These include, for example, $A_2B_4 + AB_5 = 3 \times AB_3$ [1]; $A_2B_4 + 2 \times AB_5 =$ $2 \times A_2B_7$; and $2 \times A_2B_4 + 3 \times AB_5 = A_7B_{23}$ [2]. These compounds adopt several types of structures, which are built from the slabs of Laves and Haucke types stacking along the hexagonal/trigonal c-axis.

As the A/B ratio is in the range between 1/5 and 1/2, the corresponding intermetallic hydrides exhibit intermediate properties compared to the hydrogenated AB_5 and AB_2 alloys. The structures of the hydrides of the hybrid intermetallic compounds have been studied in detail for representatives belonging to different structure types, including PuNi$_3$ ([3] and references therein), CeNi$_3$ [1], and Ce$_2$Ni$_7$ [4–6]. The formation of the hydrides is accompanied by either isotropic or anisotropic expansion of the unit

cells. This expansion reaches $\Delta a/a = 7.2$, $\Delta c/c = 9.7\%$ (LaY$_2$Ni$_9$D$_{12.8}$ [7]) for isotropic and $\Delta a/a = -1.2$, $\Delta c/c = 30.7\%$ (CeNi$_3$D$_{2.8}$ [1]) for anisotropic hydrides.

Recently, it has been found that Mg-substituted La$_{1-x}$Mg$_x$Ni$_3$ alloys ($x < 0.7$) [8,9] possess higher H discharge capacities compared to the AB_5-based hydrides [10] which makes these alloys promising metal hydride electrode materials for Ni-MH rechargeable batteries. Studies of the isothermal cross-section of the La–Mg–Ni ternary system [11] revealed that, similar to LaNi$_3$, Mg also can substitute for La in La$_2$Ni$_7$. The solubility range of Mg in La$_2$Ni$_7$ at 500 °C is rather low (up to a composition of La$_{1.75}$Mg$_{0.25}$Ni$_7$ [11]) compared to LaNi$_3$, where 2/3 of La can be replaced by Mg to reach a composition of La$_{0.33}$Mg$_{0.67}$Ni$_3$. However, Mg solubility dramatically increases at higher temperatures. The formation of a single-phase La$_{1.5}$Mg$_{0.5}$Ni$_7$ compound was achieved by a stepwise sintering complemented by annealing at 750 °C [3] or by the annealing at 900 °C of the alloy obtained by induction melting [12].

The magnesium-substituted AB_3/A_2B_7-related alloys have been studied in detail; however, information on the thermodynamics and crystal structures of their corresponding hydrides is still not available. This work is focused on the synchrotron X-ray diffraction (SR XRD) and powder neutron diffraction (PND) study of the crystal structure of La$_{1.5}$Mg$_{0.5}$Ni$_7$D$_9$ and thermodynamic properties of the La$_{1.5}$Mg$_{0.5}$Ni$_7$–H$_2$ system.

2. Experimental

2.1. Preparation of the alloy and its hydride and deuteride

The La$_{1.5}$Mg$_{0.5}$Ni$_7$ alloy was prepared by a stepwise sintering (in the temperature range 600–980 °C) of a pellet prepared from the crushed LaNi$_{4.67}$ intermetallic alloy and Mg powder (purity grade 99.9%; mesh size 100). In order to compensate for loss by evaporation during the sintering, an excess of 10 at% Mg was added. Afterwards the sintered LaNi$_{4.67}$ + Mg pellet was annealed at 750 °C for 4 days with subsequent quenching into a mixture of ice and water. The details of the preparation of the alloy are given in [3].

The prepared alloy has been characterised by the synchrotron XRD (BM01A, $\lambda = 0.7243(1)$ Å, SNBL/ESRF) and high-flux PND (SLAD instrument, $\lambda = 1.116(1)$ Å, NFL, Studsvik), which showed no detectable amounts of impurity phases present in the sample.

The hydride/deuteride of the La$_{1.5}$Mg$_{0.5}$Ni$_7$ single-phase alloy has been synthesised by gas-charging of the alloy with hydrogen (99.999% purity grade) or with deuterium (98%). The sample had been previously activated by heating in vacuum up to 350 °C. The sample for SR XRD measurements of the hydride was synthesised *in situ* in a silica capillary by applying 1.2 MPa hydrogen gas. The deuteride was synthesised *in situ* in the stainless steel tube (wall thickness 0.2 mm, $d_{inner} = 6$ mm) which was used for the PND measurements. The sample, crushed in the inert

atmosphere glove box, was placed into the tube, activated by heating in vacuum to 350 °C and then deuterated by adding 0.5 MPa deuterium.

2.2. Neutron powder diffraction

PND data for the deuterides were collected at the R2 reactor at the Studsvik Neutron Research Laboratory using the high-resolution R2D2 instrument ($\lambda = 1.551(1)$ Å, 2Θ step 0.05°) [13]. After the measurements, the deuteride was reloaded into a vanadium can ($d_{inner} = 5$ mm), sealed with indium wire; handling of the sample was performed in the glove box filled with purified argon. Subsequently, PND data were collected again for the "*ex situ*" sample.

The crystal structure of La$_{1.5}$Mg$_{0.5}$Ni$_7$D$_{9.1}$ was derived from Rietveld profile refinements of the SR XRD and PND data using the GSAS software [14]. Neutron scattering lengths ($b_{La} = 8.24$ fm; $b_{Ni} = 10.30$ fm; $b_{Mg} = 5.38$ fm; $b_D = 6.67$ fm) are taken from the GSAS library.

2.3. Measurements of the pressure–composition–temperature (PCT) relationships

The deuteride after the PND experiments has been decomposed by thermodesorption in vacuum and was used for measurements of the PCT relationships for the La$_{1.5}$Mg$_{0.5}$Ni$_7$–H$_2$ system by application of Sieverts' method. The sample was activated in vacuum at 350 °C for 1 h, cooled under vacuum to 25 °C and then slowly charged with hydrogen gas ($P_{H_2} = 1$ MPa). To achieve reproducible kinetics of hydrogen uptake and release, several absorption–desorption cycles were performed before measuring the isotherms. The purity grade of the hydrogen gas used was 99.999%. The measurements of the isotherms were performed in the temperature range 25–75 °C and at hydrogen pressures from 2×10^{-3} to 2 MPa. The equilibrium state was considered to be reached when the pressure changes became less than 10^{-5} MPa.

3. Results and discussion

3.1. Crystal structure of the La$_{1.5}$Mg$_{0.5}$Ni$_7$ alloy

A combined refinement of PND and SR XRD data for the initial La$_{1.5}$Mg$_{0.5}$Ni$_7$ intermetallic alloy concluded that it crystallises with the Ce$_2$Ni$_7$-type of hexagonal structure (space group $P6_3/mmc$). Substitution of La by Mg leads to a significant contraction of the unit cell from $a = 5.058$ Å, $c = 24.71$ Å; $V = 547.47$ Å^3 for La$_2$Ni$_7$ [15] to $a = 5.0285(2)$ Å, $c = 24.222(2)$ Å; $V = 530.42(4)$ Å^3 for La$_{1.5}$Mg$_{0.5}$Ni$_7$. The crystallographic data are provided in Table 1; SR XRD and NPD patterns are given in Fig. 1.

La substitution by Mg proceeds exclusively inside the Laves-type AB_2 slabs (site $4f_1$). After Mg substitution, the Laves-type slab has the composition LaMgNi$_4$. Because of the large difference in the atomic radii of La (1.877 Å) and Mg (1.602 Å), the Mg-containing LaMgNi$_4$ layer strongly

Table 1
Crystal structure data for metal matrix in the $La_{1.5}Mg_{0.5}Ni_7$ intermetallic compound and $La_{1.5}Mg_{0.5}Ni_7H_{9.3}$ hydride

Atom	Site	$La_{1.5}Mg_{0.5}Ni_7$					$La_{1.5}Mg_{0.5}Ni_7H_{9.3}$ (1.2 MPa H_2)				
		x	y	z	U_{iso} (10^{-2} Å^2)	Occupancy	x	y	z	U_{iso} (10^{-2} Å^2)	Occupancy
La1	$4f_1$	$\frac{1}{3}$	$\frac{2}{3}$	0.0246(2)	0.53(7)	0.498(17)	$\frac{1}{3}$	$\frac{2}{3}$	0.0166(3)	3.0(3)	0.516(11)
Mg1	$4f_1$	$\frac{1}{3}$	$\frac{2}{3}$	0.0246(2)	0.53(7)	0.502(17)	$\frac{1}{3}$	$\frac{2}{3}$	0.0166(3)	3.0(3)	0.484(11)
La2	$4f_2$	$\frac{1}{3}$	$\frac{2}{3}$	0.1701(2)	0.88(5)	1.0(–)	$\frac{1}{3}$	$\frac{2}{3}$	0.1751(2)	4.3(1)	1.0(–)
Ni1	$2a$	0	0	0	0.7(1)	1.0(–)	0	0	0	1.85(6)	1.0(–)
Ni2	$4e$	0	0	0.1656(2)	1.80(9)	1.0(–)	0	0	0.1619(3)	1.85(6)	1.0(–)
Ni3	$4f$	$\frac{1}{3}$	$\frac{2}{3}$	0.8335(2)	0.07(4)	1.0(–)	$\frac{1}{3}$	$\frac{2}{3}$	0.8275(3)	1.85(6)	1.0(–)
Ni4	$6h$	0.8337(5)	0.6675(10)	$\frac{1}{4}$	0.47(5)	1.0(–)	0.8285(9)	0.6570(18)	$\frac{1}{4}$	1.85(6)	1.0(–)
Ni5	$12k$	0.8336(4)	0.6673(7)	0.08391(6)	1.37(5)	1.0(–)	0.8331(6)	0.6662(12)	0.0858(1)	1.85(6)	1.0(–)

The data are based on combined Rietveld refinements of the SR XRD and PND data ($La_{1.5}Mg_{0.5}Ni_7$) and SR XRD ($La_{1.5}Mg_{0.5}Ni_7H_{9.3}$).
$La_{1.5}Mg_{0.5}Ni_7$: Space group $P6_3/mmc$; $a = 5.0285(2)$ Å, $c = 24.222(2)$ Å; $V = 530.42(4)$ Å^3.
$La_{1.5}Mg_{0.5}Ni_7H_{9.3}$: Space group $P6_3/mmc$; $a = 5.4121(1)$ Å, $c = 26.589(1)$ Å; $V = 674.48(4)$ Å^3.
R-factors: Alloy. SR XRD: $R_{wp} = 5.46\%$; $R_p = 4.56\%$; PND: $R_{wp} = 5.08\%$; $R_p = 3.44\%$; Combined: $R_{wp} = 5.11\%$; $R_p = 4.13\%$; $\chi^2 = 2.98$.
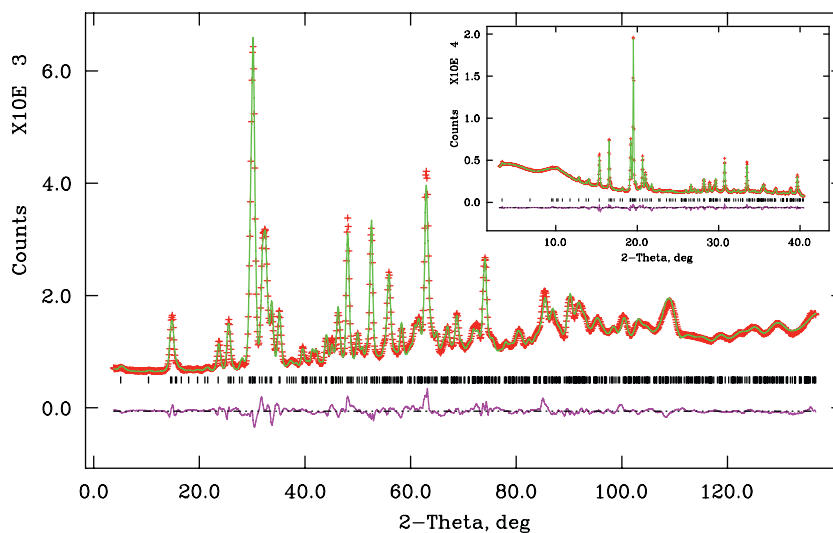Hydride. SR XRD: $R_{wp} = 4.03\%$; $R_p = 2.99\%$; $\chi^2 = 2.32$.

Fig. 1. Observed (+), calculated (upper line) and difference (lower line) profiles of the $La_{1.5}Mg_{0.5}Ni_7$ alloy: powder neutron diffraction (SLAD instrument, $\lambda = 1.116(1)$ Å). Inset: synchrotron X-ray diffraction (SNBL, BM01A, $\lambda = 0.7243(1)$ Å).

contracts (see Table 2) compared to the initial La_2Ni_4 slab. Due to the contraction of the basal plane of the unit cell, the adjacent $LaNi_5$ layer contracts as well but by less than 1%. The stacking of the slabs to form the crystal structure is shown in Fig. 2.

The structure of the $LaNi_5$ layer may be described as composed of two kinds of slabs with the $LaNi_5$ stoichiometry: the "outer" $LaNi_5$ slab connected to the $LaMgNi_4$ slab, and an "inner" $LaNi_5$ slab sandwiched in between two "outer" $LaNi_5$ ones. The combination $LaMgNi_4 + 2 \times LaNi_5$ gives an overall stoichiometry La_3MgNi_{14} ($2 \times La_{1.5}Mg_{0.5}Ni_7$). The "inner" AB_5-type layer is bordered above and below by the nets containing the La2 atoms; two identical "outer" parts are located above and below this "inner" part. The "outer" layers have a larger volume compared to the "inner" ones (see Table 2). The

significant difference between the $LaNi_5$ layers is introduced by ordered Mg substitution for La. The external, "outer", $LaNi_5$ layer contains a number of interstitial sites formed with participation of Mg from the adjacent Laves-type $LaMgNi_4$ layer. With Mg substitution the volume of the $LaMgNi_4$ slab has decreased the most (−7.62%) compared with La_2Ni_7. The bordering "outer" $LaNi_5$ layer becomes contracted by −0.95%, whereas the central "inner" $LaNi_5$ slab is the least contracted compared to La_2Ni_7 (−0.38%) as this slab is the most distant from the Mg sites.

3.2. Thermodynamic (PCT) measurements

The single plateau behaviour is clearly seen in the absorption and desorption isotherms (Fig. 3). The two-phase

Table 2
Comparison of crystallographic parameters of La–Ni A_2B_7 compounds and their hydrides

Compound	La$_2$Ni$_7$ [15]	La$_2$Ni$_7$D$_{6.5}$ [4]	La$_{1.5}$Mg$_{0.5}$Ni$_7$	La$_{1.5}$Mg$_{0.5}$Ni$_7$D$_{9.1}$	La$_{1.5}$Mg$_{0.5}$Ni$_7$D$_{8.9}$
a (Å)	5.058	4.9534	5.0285	5.3991	5.3854
c (Å)	24.71	29.579	24.222	26.543	26.437
V (Å^3)	547.47	628.52	530.42	670.07	664.01
d_{AB_5} (inner) (Å)[a]	3.970	3.861	4.001	4.396	4.381
d_{AB_5} (outer) (Å)[a]	4.036	4.232	4.045	4.300	4.237
$d_{A_2B_4}$ (Å)	4.349	6.697	4.065	4.576	4.600
V_{AB_5} (inner) (Å^3)	87.96	82.04	87.62	110.96	110.05
V_{AB_5} (outer) (Å^3)	89.42	89.92	88.57	108.55	106.42
$V_{A_2B_4}$ (Å^3)	96.35	142.30	89.01	115.52	115.54
$\Delta a/a$ (%)[b]	–	−2.07	**−0.58**	7.37	7.10
$\Delta c/c$ (%)[a]	–	19.70	**−1.97**	9.58	9.14
$\Delta V/V$ (%)	–	14.8	**−3.1**	26.3	25.2
ΔV_{AB_5} (inner) (%)	–	−6.73	**−0.38**	26.64	25.59
ΔV_{AB_5} (outer) (%)	–	0.56	**−0.95**	22.56	20.15
$\Delta V_{A_2B_4}$ (%)	–	47.68	**−7.62**	29.78	29.80

[a]The separation between two types of the AB_5 layers is made along the buckled net containing the La2, Ni2 and Ni3 atoms.
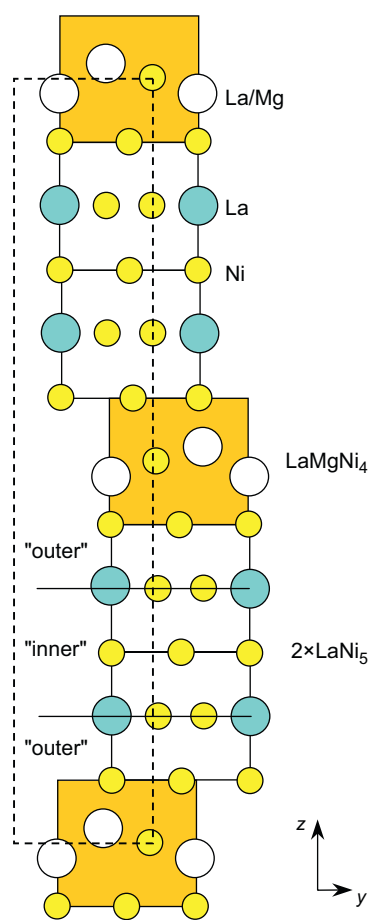[b]The changes of the crystallographic parameters due to partial Mg substitution for La are shown in bold type.

Fig. 2. Structure of La$_{1.5}$Mg$_{0.5}$Ni$_7$ intermetallic compound as a stacking of MgZn$_2$-type (shaded) and CaCu$_5$-type slabs.

region is observed at H content $1 < $[H]$/$[La$_{1.5}Mg_{0.5}Ni_7$]$ < 8$. The isotherms are not horizontal; their slope becomes higher with an increase of temperature. The observed hysteresis P_{abs}/P_{des} is typical; its value of 1.4 is higher than that for the chemically similar Ce$_2$Ni$_7$H$_{4.7}$ [5]. Based on the measured PCT diagrams, the changes in the relative partial molar enthalpy ΔH_H and entropy ΔS_H were calculated for H$_2$ absorption and desorption at [H]$/$[La$_{1.5}$Mg$_{0.5}$Ni$_7$] $= 5$ from the van't Hoff relation. The values obtained are $\Delta H_H = -15.7 \pm 0.9\,\text{kJ}(\text{mol}_H)^{-1}$ and $\Delta S_H = -46.0 \pm 3.7\,\text{J}(\text{K mol}_H)^{-1}$ for H$_2$ absorption, and $\Delta H_H = 16.8 \pm 0.4\,\text{kJ}(\text{mol}_H)^{-1}$ and $\Delta S_H = 48.1 \pm 1.5\,\text{J}(\text{K mol}_H)^{-1}$ for H$_2$ desorption.

The increase in Mg content in La$_{1-x}$Mg$_x$Ni$_3$ ($x \leqslant 0.67$) leads to a gradual decrease in the hydrogenation capacity [16]. In this work, the observed hydrogenation capacity of H$/$La$_{1.5}$Mg$_{0.5}$Ni$_7$ = 9 at 298 K is just slightly lower than that observed for the La$_2$Ni$_7$–H$_2$ system (H$/$La$_2$Ni$_7$ = 10 at 263 K). However, we note the dramatic increase of the reversible hydrogenation capacity (>7 at.H/f.u.; about 90% of capacity). In La$_2$Ni$_7$–H$_2$ system the reversible capacity is lower, being limited to 5 H$/$La$_2$Ni$_7$; hydrogen absorption–desorption cycling in this system seems to be accompanied by hydrogen-induced disproportionation. Similar observations have been made by Oesterreicher et al. [17], who noticed that La$_2$Ni$_7$H$_{10}$ decomposes with hydrogen desorption. Such disproportionation also made impossible measurements of the thermodynamic data for the chemically related LaNi$_3$–H and LaNi$_2$–H systems, where hydrides easily become amorphous and, later, disproportionate.

The comparison of the present results with the available data for hydrides of AB_3, A_2B_7 and AB_2 intermetallic compounds supports the conclusion that in all anisotropic hydrides, ΔH is in a rather narrow range of values, −22 to −23 kJ$(\text{mol}_H)^{-1}$ neglecting the chemical nature of the constituent elements (see Table 2 in [5]), whereas the value for the hydride formation enthalpy, $-15.7 \pm 0.9\,\text{kJ}(\text{mol}_H)^{-1}$ obtained in this work is close to that obtained for the LaNi$_5$–H system, $-15.8\,\text{kJ}(\text{mol}_H)^{-1}$ [18]. Such a similarity
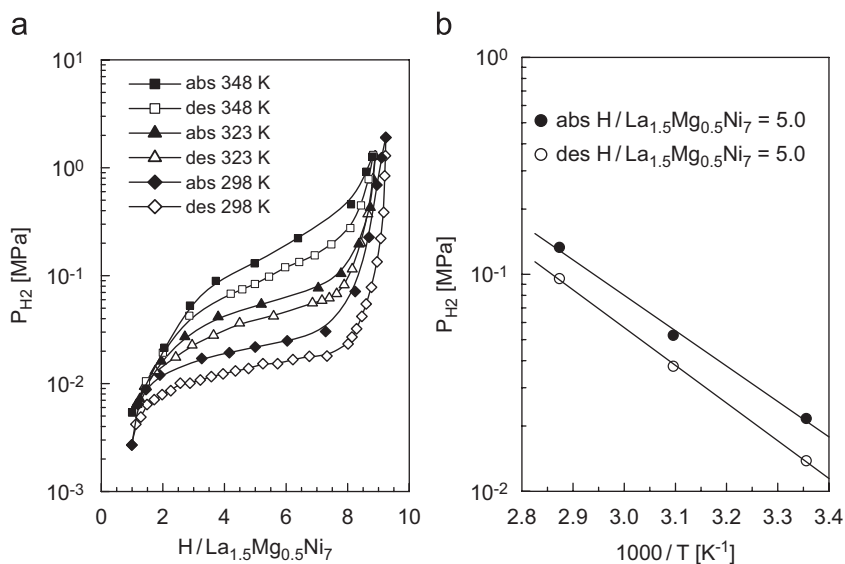
Fig. 3. PCT measurements for the $La_{1.5}Mg_{-0.5}Ni_7$–H_2 system: H_2 absorption–desorption isotherms (a) and vant' Hoff dependences $\log P_{H2}$ vs. $1/T$ (b).

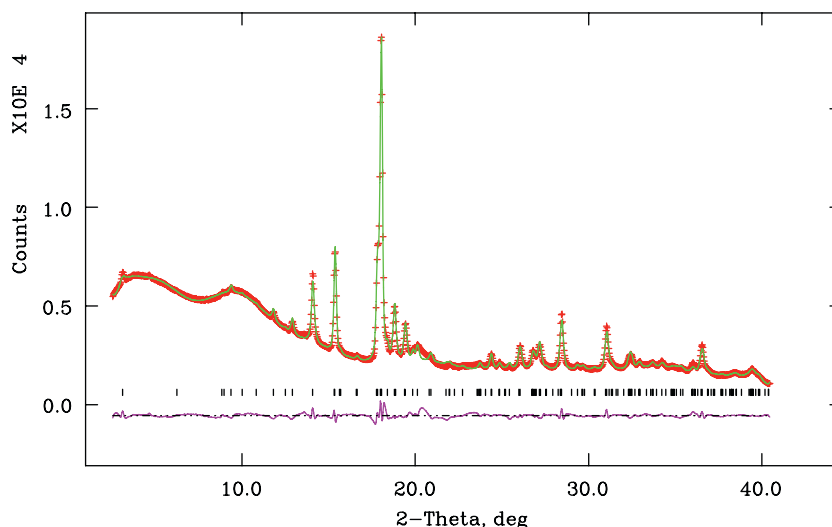
Fig. 4. Observed (+), calculated (upper line) and difference (lower line) profiles during *in situ* SR XRD experiment (1.2 MPa H_2) of the $La_{1.5}Mg_{0.5}Ni_7H_{9.3}$ hydride.

supports the conclusion that $La_{1.5}Mg_{0.5}Ni_7$ hydride belongs to conventional, interstitial type hydrides, represented by $LaNi_5H_{\sim 6}$.

3.3. SR XRD study of the hydride

The *in situ* hydrogenation of the $La_{1.5}Mg_{0.5}Ni_7$ alloy under 1.2 MPa hydrogen gas resulted in the formation of the hydride with the composition of $La_{1.5}Mg_{0.5}Ni_7H_{9.3}$, as follows from the PCT isotherm at 298 K (Fig. 3). The hydrogenation is accompanied by isotropic expansion of the unit cell, $\Delta a/a = 7.63\%$, $\Delta c/c = 9.77\%$. These values are close to those observed for the formation of the $LaY_2Ni_9D_{12.8}$ deuteride of the filled $PuNi_3$ type of structure [7] and are in sharp contrast with the values for

the hydride of the isostructural non-substituted La_2Ni_7 alloy, which expands anisotropically [4] (see Table 2). The isotropic expansion of the unit cell of $La_{1.5}Mg_{0.5}Ni_7$ indicates that the hydrogenation leads to an even distribution of hydrogen through all the slabs of the structure, similarly as it has been observed for $LaY_2Ni_9D_{12.8}$ [7]. This is in contrast to anisotropic hydrides, where only Laves phase-type slabs accommodate hydrogen, leaving the $CaCu_5$-type layers unexpanded.

Refinements of the SR XRD data (Fig. 4 and Table 1) showed that Mg ordering within two types of the available $4f$ R-sites did not change with hydrogenation; only one type of sites (1/3, 2/3, 0.0166(3)) located inside the Laves-type slab was statistically and equally filled by La or Mg. The structure of the metal matrix as refined on the basis of

SR XRD data have been used as a starting point in the course of refinement of the PND data.

3.4. PND of deuterides

The Rietveld plots of the calculated and observed PND intensity data for the *in situ* and *ex situ* samples are shown in Fig. 5. The refinement results are given in Table 3; selected interatomic distances in the structures of $La_{1.5}Mg_{0.5}Ni_7D_{9.1}$ and $La_{1.5}Mg_{0.5}Ni_7D_{8.9}$ are provided in Table 4. Similar to the structure of the hydride described above, the formation of the deuteride is accompanied by an isotropic expansion of the unit cell, reaching values of $\Delta a/a = 7.37\%$, $\Delta c/c = 9.58\%$ for *in situ* and $\Delta a/a = 7.10\%$, $\Delta c/c = 9.14\%$ for the *ex situ* measurements. The positions

of the deuterium have been determined by the use of Fourier synthesis after introduction of positions of the metallic atoms taken from the refinement of the SR XRD data for the hydride. The deuterium positions are situated inside the $(La,Mg)_2Ni_2$, $(La,Mg)Ni_3$ and Ni_4 tetrahedra; La_2Ni_3 tetragonal pyramids and $(La,Mg)_3Ni_2$ trigonal bipyramids (for details see Table 4 and Fig. 6). As follows from the comparison of refinement results for the *in situ* and *ex situ* data sets, the release of deuterium pressure leads to the slight decrease of deuterium content from 9.1 to 8.9 D/f.u. and is accompanied with a small contraction of the unit cell from $\sim$670 to $\sim$664 $Å^3$. The hydrogenation capacities of both *in situ* and *ex situ* samples agree well with the hydrogen desorption isotherm at 298 K in the $La_{1.5}Mg_{0.5}Ni_7–H_2$ system.
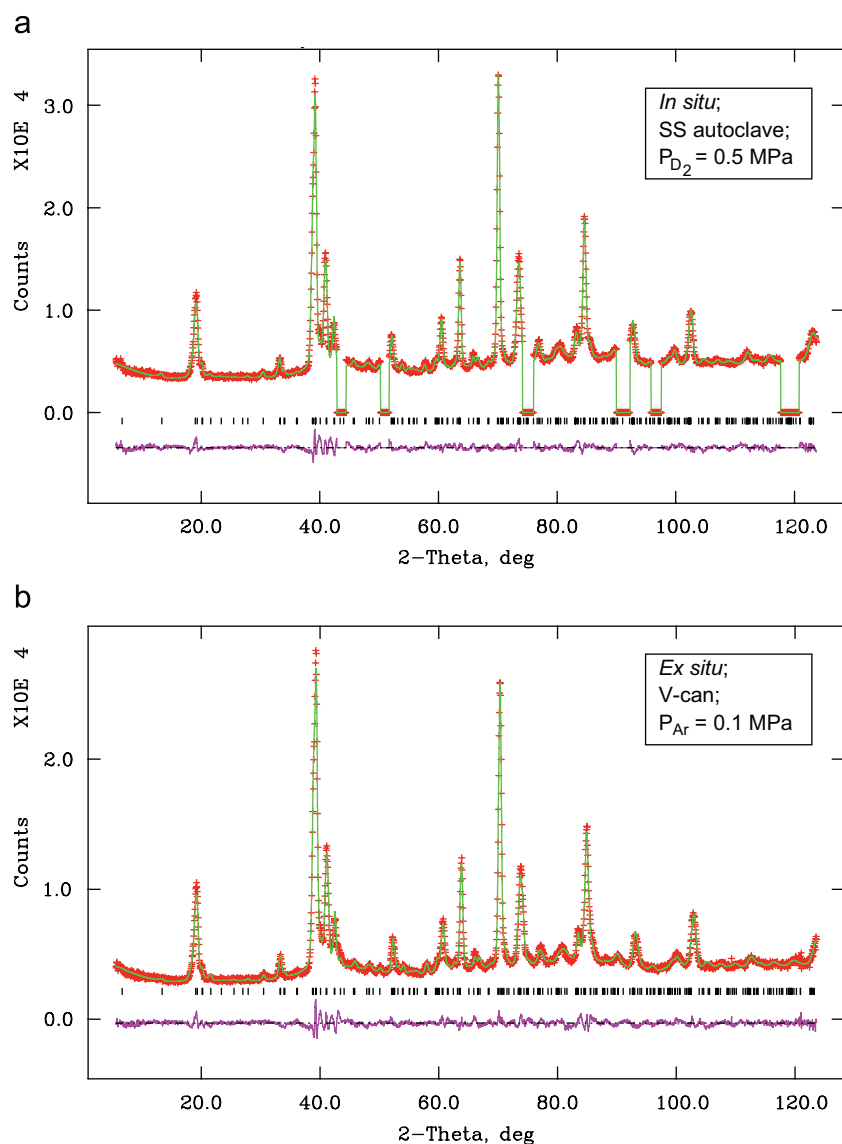

Fig. 5. Observed (+), calculated (upper line) and difference (lower line) PND profiles of the $La_{1.5}Mg_{0.5}Ni_7$-based deuterides ($\lambda = 1.551(1)\,Å$): (a) *in situ* data collected for $La_{1.5}Mg_{0.5}Ni_7D_{9.1}$ at applied pressure of 0.5 MPa D_2 (2Θ ranges where contributions from the stainless steel autoclave were observed, 43.2–44.2; 50.35–51.55; 73.85–75.85; 90.35–92.5; 95.8–97.3 and 118.05–120.2, were excluded from the refinements); (b) *ex situ* data collected for $La_{1.5}Mg_{0.5}Ni_7D_{8.9}$.

Table 3
Atomic parameters in the structure of $La_{1.5}Mg_{0.5}Ni_7$-based deuterides from Rietveld refinements of the powder neutron diffraction data

Lattice parameters (Å)	Site	$La_{1.5}Mg_{0.5}Ni_7D_{9.1}$ $a = 5.3991(1)$ $c = 26.543(2)$				$La_{1.5}Mg_{0.5}Ni_7D_{8.9}$ $a = 5.3854(1)$ $c = 26.437(2)$			
Atom	Site	x	y	z	Occ.	x	y	z	Occ.
La1	4f	$\frac{1}{3}$	$\frac{2}{3}$	0.0169(5)	0.50(–)	$\frac{1}{3}$	$\frac{2}{3}$	0.0160(5)	0.50(–)
Mg1	4f	$\frac{1}{3}$	$\frac{2}{3}$	0.0169(5)	0.50(–)	$\frac{1}{3}$	$\frac{2}{3}$	0.0160(5)	0.50(–)
La2	4f	$\frac{1}{3}$	$\frac{2}{3}$	0.1723(6)	1.0(–)	$\frac{1}{3}$	$\frac{2}{3}$	0.1735(5)	1.0(–)
Ni1	2a	0	0	0	1.0(–)	0	0	0	1.0(–)
Ni2	4e	0	0	0.1603(4)	1.0(–)	0	0	0.1603(4)	1.0(–)
Ni3	4f	$\frac{1}{3}$	$\frac{2}{3}$	0.8314(4)	1.0(–)	$\frac{1}{3}$	$\frac{2}{3}$	0.8323(4)	1.0(–)
Ni4	6h	0.843(1)	0.686(2)	$\frac{1}{4}$	1.0(–)	0.841(1)	0.682(2)	$\frac{1}{4}$	1.0(–)
Ni5	12k	0.8350(6)	0.670(1)	0.0863(2)	1.0(–)	0.8366(6)	0.673(1)	0.0869(2)	1.0(–)
D1	12k	0.310(3)	0.155(1)	0.1800(5)	0.40(1)	0.306(3)	0.153(1)	0.1809(5)	0.371(9)
D2	6h	0.512(1)	0.488(1)	$\frac{1}{4}$	0.77(3)	0.509(1)	0.491(1)	$\frac{1}{4}$	0.82(2)
D3	4e	0	0	0.2186(7)	0.50(–)	0	0	0.2176(6)	0.50(–)
D4	12k	0.342(4)	0.171(2)	0.1419(4)	0.46(1)	0.346(4)	0.173(2)	0.1438(4)	0.492(9)
D5	12k	0.174(3)	0.348(6)	0.0892(6)	0.32(1)	0.166(3)	0.332(6)	0.0942(7)	0.28(1)
D6	12k	0.484(2)	0.516(2)	0.0885(7)	0.40(2)	0.480(2)	0.520(2)	0.0878(7)	0.39(2)
D7	12k	0.306(2)	0.153(1)	0.0250(4)	0.50(2)	0.292(2)	0.146(1)	0.0240(4)	0.46(2)
D8	12k	0.527(2)	0.473(2)	0.4461(9)	0.31(2)	0.533(1)	0.467(1)	0.4494(8)	0.29(2)
D9	4f	$\frac{2}{3}$	$\frac{1}{3}$	0.068(1)	0.27(2)	$\frac{2}{3}$	$\frac{1}{3}$	0.073(1)	0.27(2)
		U_{iso} $(10^{-2}$ Å$^2)^a$				U_{iso} $(10^{-2}$ Å$^2)^a$			
La(Mg)		3.1(2)				2.3(2)			
Ni		2.59(6)				2.87(6)			
D		1.0(2)				1.1(1)			
R-factors		$R_{wp} = 3.88\%$; $R_p = 3.23\%$; $\chi^2 = 4.95$				$R_{wp} = 4.02\%$; $R_p = 3.43\%$; $\chi^2 = 4.33$			

[a] U_{iso} parameters have been constrained to be equal for the chemically and structurally identical groups of atoms: La1, Mg1 and La2; Ni1–Ni5; D1–D9.

3.5. Structure analysis of $La_{1.5}Mg_{0.5}Ni_7D_{9.1}$

We will present here the detailed analysis of the structure of the deuteride based on refinement results of the in situ data ($La_{1.5}Mg_{0.5}Ni_7D_{9.1}$).

The hydrogenation/deuteration leads to the expansion of all three types of slabs, which, however, varies from a minimum 22.56% for the "outer" $LaNi_5$ sub-slab to maximum 29.78% for the $LaMgNi_4$ slab (Table 2). In agreement with larger expansion (26.64% for the "inner" $LaNi_5$ slab), a much higher hydrogen content (5.71 at.D/f.u.) is observed for this internal layer.

3.5.1. $LaNi_5$ slabs

The hydrogen sublattice in the "inner" layer $LaNi_5D_{5.71}$ is formed by hydrogen occupation of the following sites (to simplify the comparison we use notation of sites as that for the $CaCu_5$-type Haucke structure; space group $P6/mmm$): 1.0 D in $Ni_4/4e$; 2.30 D in $La_2Ni_2/6m$; and 2.41 D in $LaNi_3/12n$. This sublattice is essentially the same as reported for $LaNi_5D_{6.37}$ [19] (0.95 D in $4e$; 3.00 D in $6m$; 2.42 D in $12n$).

Due to the proximity of the "outer" $LaNi_5$ slab to the Mg-containing $LaMgNi_4$ layer, the former expands less than the "inner" $LaNi_5$ slab and accommodates 4.92 at.D/$LaNi_5$ (2.12 D in $6m + 2.76$ D in $12n$); the Ni_4 $4e$ site

remains unoccupied. The hydrogen sublattice in this layer is similar to that of the structure of the $LaNi_5D_{5.52}$ deuteride [20]. The introduction of Mg decreases the overall D content in the AB_5 layer from 5.71 to 4.92 at.D/f.u.; however, the occupancy of the interstitial sites formed by Mg replacement increases as compared to the original La-neighbouring sites. In contrast, the Ni_4 sites become completely unoccupied by D. No D-ordering is observed in neither the "inner" nor "outer" $LaNi_5$ slabs. The La atoms inside the $LaNi_5$ layer are surrounded by a 21-vertex polyhedron of D-sites, of which only 12 can be occupied simultaneously when considering the limitations imposed by D⋯D blocking for very short D interatomic distances (Fig. 7c).

3.5.2. $LaMgNi_4$ slab

The main feature of the $MgZn_2$-type $LaMgNi_4$ slab is the occupancy of all four available types of the R_2Ni_2 sites that are $6h_1$, $6h_2$, $12k_1$ and $24l$ sites according to the notation adopted for the $MgZn_2$-type hydrides [21]. D occupies simultaneously these four types of sites in the structures of $ZrMn_2D_{2.76}$ [22], $ScFe_2D_{2.53}$ [23], and $Ti_{1.2}Mn_{1.8}D_{3.1}$ [24]. In addition to $(La,Mg)_2Ni_2$, one of the RNi_3 sites, $4f$, is also occupied also as is observed in the structure of $ZrVFeD_{3.6}$ [21]. The $(La,Mg)_2Ni_2$ sites are preferably filled

Table 4
Selected interatomic distances (Å) in the crystal structures of $La_{1.5}Mg_{0.5}Ni_7$-based deuterides

Atoms	Interstitial site	$La_{1.5}Mg_{0.5}Ni_7D_{9.1}$	$La_{1.5}Mg_{0.5}Ni_7D_{8.9}$
D1···2 La2	Tetragonal pyramid $La_2Ni2Ni3Ni4$	2.709(2)	2.703(2)
D1···Ni2		1.54(1)	1.52(1)
D1···Ni3		1.70(1)	1.72(1)
D1···Ni4		1.86(1)	1.83(1)
D1···D3		1.77(2)	1.72(2)
D1···D4		1.02(1)	1.00(1)
D2···2 La2	Tetrahedron La_2Ni4_2	2.65(1)	2.61(1)
D2···2 Ni4		1.556(6)	1.551(5)
D3···Ni2	Tetrahedron $Ni2Ni4_3$	1.55(2)	1.52(2)
D3···3 Ni4		1.69(1)	1.72(1)
D3···3 D1		1.77(2)	1.72(2)
D3···D3		1.67(4)	1.71(3)
D4···2 La2	Tetragonal pyramid $La_2Ni2Ni3Ni5$	2.818(5)	2.805(4)
D4···Ni2		1.67(2)	1.67(2)
D4···Ni3		1.68(2)	1.63(2)
D4···Ni5		1.48(1)	1.51(1)
D4···D1		1.02(1)	1.00(1)
D5···(La,Mg)1	Tetrahedron $(La,Mg)1La2Ni5_2$	2.43(2)	2.59(2)
D5···La2		2.66(2)	2.62(3)
D5···2 Ni5		1.59(1)	1.55(1)
D5···D6		1.45(1)	1.49(1)
D6···(La,Mg)1	Tetrahedron $(La,Mg)1La2Ni5_2$	2.36(2)	2.34(2)
D6···La2		2.63(2)	2.65(2)
D6···2 Ni5		1.65(1)	1.667(8)
D6···D5		1.45(1)	1.49(1)
D6···D8		1.01(2)	1.10(3)
D6···D9		1.79(2)	1.78(2)
D7···2 (La,Mg)1	Trigonal bypyramid $(La,Mg)1_3Ni1Ni5$	2.711(2)	2.708(2)
D7···(La,Mg)1		2.02(1)	2.041(9)
D7···Ni1		1.58(1)	1.50(1)
D7···Ni5		1.63(1)	1.67(1)
D7···2 D7		1.96(2)	1.86(2)
D7···2 D8		1.71(1)	1.71(1)
D8···(La,Mg)1	Tetrahedron $(La,Mg)1_2Ni5_2$	2.29(3)	2.16(3)
D8···(La,Mg)1		2.06(1)	2.08(1)
D8···2 Ni5		1.69(1)	1.74(1)
D8···D6		1.00(2)	1.10(3)
D8···2 D7		1.71(1)	1.71(1)
D8···D9		1.36(2)	1.38(2)
D9···(La,Mg)1	Tetrahedron $(La,Mg)1Ni5_3$	2.26(3)	2.34(4)
D9···3 Ni5		1.65(1)	1.63(1)
D9···3 D6		1.79(2)	1.78(2)
D9···3 D8		1.36(2)	1.38(2)

Table provides the values of the "blocking" distances between neighbouring D positions (1.0–1.9 Å). Due to partial occupancy of D sites the "blocked" sites are never simultaneously filled; minimum distance between neighbouring D atoms in the structure exceeds 1.9 Å.

(93% from overall hydrogenation capacity of 7.56 at.D/ $LaMgNi_4$). For the 24*l* sites, the D atoms are shifted into a common triangular $(Mg/La)Ni_2$ face, which makes this deuterium position co-ordinated by a trigonal bipyramid $(Mg/La)_3Ni_2$.

Similar to the structures of the hydrides of $MgZn_2$-type intermetallics the hydrogen sublattice within the $LaMgNi_4$ slab is not ordered. This is in contrast with the structure of $La_2Ni_7D_{6.5}$ where all D···D distances are larger than 1.8 Å, and the deuterium sublattice is completely ordered. In the latter case the capacity of the $MgZn_2$-type layer corresponds to $LaNi_2D_5$, which is significantly higher than the capacity of the $LaMgNi_4$ slab. This agrees with the values of the expansion of the layers, which are 47.68% and 29.78%, respectively (Table 2).

3.5.3. Deuterium sublattice

The R-site inside the $LaMgNi_4$ slab has an equal probability to be occupied by Mg or La. There are 22 partly occupied D-sites around the R-site; of these six are at distances of 2.02–2.06 Å and 16—at 2.25–2.71 Å. Accounting for the substantial difference in atomic radii of Mg and La, we can consider that the distances of 2.02–2.06 Å correspond to an octahedron around the Mg atom, whereas a 16-vertex external polyhedron surrounds the La atom (Figs. 7a and b). In total, D atoms fill nine types of interstitial sites (Fig. 6 and Table 4). In contrast to the previously studied anisotropic $La_2Ni_7D_{6.5}$ hydride, where the hydrogen sublattice is layered and limited only to Laves-type layers, the spatial framework of hydrogen atoms extended throughout all the structure of $La_{1.5}Mg_{0.5}Ni_7D_9$ is observed. This framework is formed by polyhedra of three types: an octahedron around each Mg atom as well as 16-vertex polyhedra around the La atoms (Fig. 7). The MgD_6 octahedra sites are completely occupied by H; thus, these octahedra are completely ordered. The $La1D_{16}$ polyhedron within the $LaMgNi_4$ slab is partially ordered and could have a maximum of 12 simultaneously occupied vertices—six D7, three D8 and three either D5 or D6 sites, on the boundary between $LaMgNi_4$ and the "outer" $LaNi_5$ slabs. For the case of complete ordering of La and Mg atoms inside the $LaMgNi_4$ slab, the D9 position will remain empty, since it is blocked by three D8 atoms surrounding the Mg atoms. The previously mentioned 21-vertex $La2D_{21}$ polyhedron inside the $LaNi_5$ slab also can not have more than 12 simultaneously occupied vertices—half of twelve mutually blocking D1 and D4 sites, three D2 sites and the same type of the occupancy of the D5 and D6 sites as described for the $La1D_{16}$ polyhedron. The maximum H storage capacity based on the structure thus described is $La_{1.5}Mg_{0.5}Ni_7D_{11}$ and can be presented as $\frac{1}{2}$ ($LaNi_5D_7$ (inner) + $LaNi_5D_6$ (outer) + $LaMgNi_4D_9$). Obviously, the isotropic expansion of the unit cell is caused by the fact that all the layers, Laves-type, and both Haucke types, reach a high content of H compared to their maximum theoretical capacities.
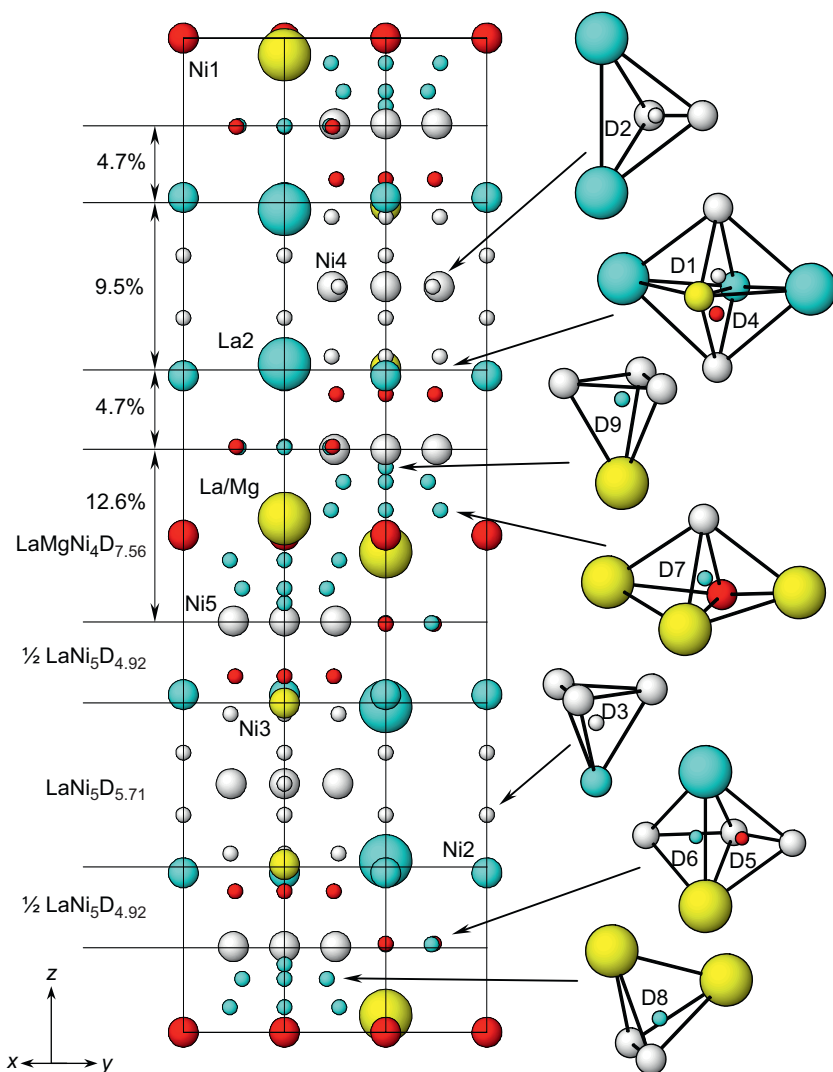
Fig. 6. Crystal structure of $La_{1.5}Mg_{0.5}Ni_7D_{9.1}$ showing the stacking of the $LaNi_5$ and $LaMgNi_4$ slabs with their relative expansion during deuteration. The coordination of each D site is shown and each site location is indicated.
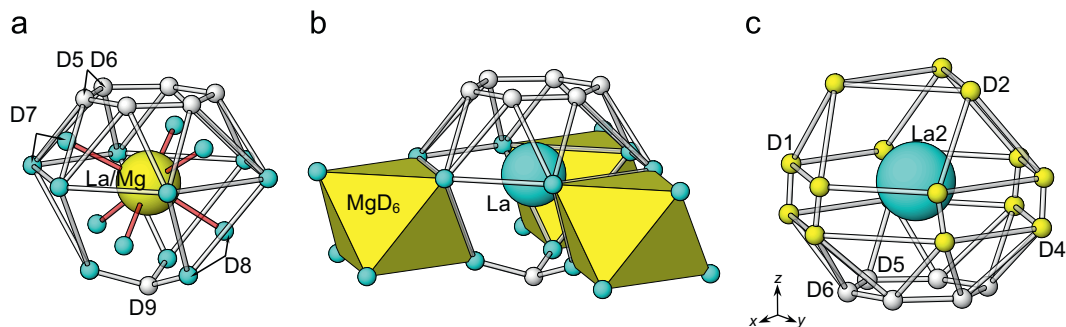

Fig. 7. (a) Hydrogen sublattice inside the $LaMgNi_4D_{7.56}$ layer. The central position is jointly occupied by La and Mg. Hydrogen sites form two different coordination spheres—an internal one, with $d_{Me-D} = 2.02$–2.06 Å, and an external sphere with much larger Me–D distances, 2.25–2.71 Å. The internal D sphere forms an octahedron around the metal atom; because of much smaller Me–D distances, this atom can only be Mg. The external sphere forms a 16-vertex polyhedron centred on La atom, LaD_{16}. (b) Assuming local ordering of Mg and La in the layer, gives packing of the MgD_6 octahedra and LaD_{16} polyhedra as shown. (c) Hydrogen sublattice inside the $LaNi_5$ layer formed by a 21-vertex polyhedron of D sites of which only 12 can be occupied simultaneously when considering the limitations imposed by D···D blocking for very short D interatomic distances.

The decrease of hydrogen content with the decrease of pressure from 0.5 to 0.1 MPa is not very substantial, only 0.25 $H/La_{1.5}Mg_{0.5}Ni_7$ as these pressures exceed the desorption plateau pressure at room temperature. The slight decrease in H content is accompanied by a moderate reduction of the unit cell volume. However, the desorption

in such a case occurs mostly from the $LaMgNi_4$ layer, which indicates that Mg reduces the affinity of this layer to hydrogen compared to that of the $LaNi_5$ layers. Interestingly, the partial release of hydrogen from the $LaMgNi_4$ layer is not accompanied by contraction of this layer (see Table 2); instead both the "inner" and "outer" $LaNi_5$ slabs slightly contract.

4. Conclusions

Our results show that Mg has an important influence on different aspects of hydrogen interaction with the $(La,Mg)_2Ni_7$ alloy.

These changes are caused by partial replacement of La by Mg inside the Laves type slabs and include:

- Increase of the reversible hydrogen storage capacity;
- Change of the mechanism of hydrogenation from an "anisotropic" hydride to an "isotropic" one;
- Absence of amorphisation and disproportionation of the metal matrix on cycling of hydrogenation and decomposition because of the stabilisation of the metal sublattice by Mg;
- Change of the thermodynamics of the metal-hydrogen interaction where smaller values of enthalpy of hydrogenation indicate formation of the interstitial type hydride.

Theoretical studies will be invaluable in gaining knowledge of the nature of the metal-hydrogen interactions in these structures. Successful synthesis of new materials will depend on the Mg-assisted ability to create new additional sites for hosting hydrogen. The present work contributes to the design of new Mg-containing materials with higher hydrogen discharge capacities for technological applications such as electrode materials in rechargeable Ni/MH batteries.

References

[1] V.A. Yartys, O. Isnard, A.B. Riabov, L.G. Akselrud, J. Alloys Compd. 356–357 (2003) 109–113.

[2] T. Kohno, H. Yoshida, F. Kawashima, T. Inaba, I. Sakai, M. Yamamoto, M. Kanda, J. Alloys Compd. 311 (2) (2000) L5–L7.

[3] R.V. Denys, A.B. Riabov, V.A. Yartys, R.G. Delaplane, M. Sato, J. Alloys Compd. 446–447 (2007) 166–172.

[4] V.A. Yartys, A.B. Riabov, R.V. Denys, M. Sato, R.G. Delaplane, J. Alloys Compd. 408–412 (2006) 273–279.

[5] R.V. Denys, V.A. Yartys, M. Sato, A.B. Riabov, R.G. Delaplane, J. Solid State Chem. 180 (9) (2007) 2566–2576.

[6] Y.E. Filinchuk, K. Yvon, H. Emerich, Inorg. Chem. 46 (7) (2007) 2914–2920.

[7] M. Latroche, V. Paul-Boncour, A. Percheron-Guégan, J. Solid State Chem. 177 (2004) 2542–2549.

[8] K. Kadir, T. Sakai, I. Uehara, J. Alloys Compd. 257 (1997) 115–121.

[9] K. Kadir, T. Sakai, I. Uehara, J. Alloys Compd. 302 (2000) 112–117.

[10] Y.J. Chai, K. Sakaki, K. Asano, H. Enoki, E. Akiba, T. Kohno, Scripta Mater. 57 (2007) 545–548.

[11] S. De Negri, M. Giovannini, A. Saccone, J. Alloys Compd. 439 (2007) 109–113.

[12] F.-L. Zhang, Y.-C. Luo, J.-P. Chen, R.-X. Yan, J.-H. Chen, J. Alloys Compd. 430 (2007) 302–307.

[13] A. Wannberg, M. Gronros, A. Mellergard, L.-E. Karlson, R.G. Delaplane, B. Lebech, Z. Kristallogr. Suppl. 23 (2006) 195–198.

[14] C. Larson, R.B. von Dreele, General structure analysis system (GSAS), LANSCE, MS-H 805, 1994.

[15] K.H.J. Buschow, A.S. van der Goot, J. Less-Common Met. 22 (4) (1970) 419–428.

[16] B. Liao, Y.Q. Ley, G.L. Lu, L.X. Chen, H.G. Pan, Q.D. Wang, J. Alloys Compd. 356–357 (2003) 476–749.

[17] H. Oesterreicher, J. Clinton, H. Bittner, Mater. Res. Bull. 11 (1976) 1241–1248.

[18] W.N. Hubbard, P.L. Rawlins, P.A. Connick, R.E. Stedwell Jr., P.A.G. O'Hare, J. Chem. Thermodyn. 15 (8) (1983) 785–798.

[19] C. Lartigue, A. Percheron-Guegan, J.C. Achard, J.L. Soubeyroux, J. Less-Common Met. 113 (1985) 127–148.

[20] D. Noréus, L.G. Olsson, P.-E. Werner, J. Phys. F: Met. Phys. 13F (1983) 715–727.

[21] V.A. Yartys, V.V. Burnasheva, N.V. Fadeeva, S.P. Solov'ev, K.N. Semenenko, Int. J. Hydrogen Energy 7 (12) (1982) 957–965.

[22] J.-J. Didisheim, K. Yvon, D. Shaltiel, P. Fischer, Solid State Commun. 31 (1979) 47–50.

[23] V.A. Yartys, V.V. Burnasheva, N.V. Fadeeva, Sov. J. Inorg. Chem. 31 (10) (1986) 2500–2503.

[24] D. Fruchart, J.L. Soubeyroux, R. Hempelmann, J. Less-Common Met. 99 (1984) 307–319.